Effects of pulse width on nascent laser-induced bubbles for underwater laser-induced breakdown spectroscopy

Tetsuo Sakka[1]*, Ayaka Tamura[1], Ayumu Matsumoto[1], Kazuhiro Fukami[2], Naoya Nishi[1], and Blair Thornton[3]

1) *Department of Energy and Hydrocarbon Chemistry, Graduate School of Engineering, Kyoto University, Nishikyo-ku, Kyoto 615-8510, Japan*

Email: sakka.tetsuo.2a@kyoto-u.ac.jp,

2) *Department of Materials Science and Engineering, Graduate School of Engineering, Kyoto University, Yoshida Honmachi, Sakyo-ku, Kyoto 606-8501, Japan*

3) *Institute of Industrial Science, The University of Tokyo, Komaba, Meguro-ku, Tokyo 153-8505, Japan*

**Corresponding author: Email: sakka.tetsuo.2a@kyoto-u.ac.jp, Phone:+81-75-383-2489, Fax:+81-75-383-2490*

Abstract

The reason for the significant advantage offered by long-pulse (150 ns) irradiation in underwater laser-induced breakdown spectroscopy (LIBS) is investigated from the point of view of the behavior of nascent cavitation bubbles. Shadowgraphs of nascent bubbles generated by pulsed laser irradiation of Cu targets in water were observed for two different pulse widths, 20 ns and 150 ns. It is clearly seen that the nascent bubble is formed at the leading edge of the laser pulse profile, regardless of the pulse width. Bubbles generated by a 20-ns pulse are characterized by a flat-shape filled with dense matter with intense optical emission, which is in contrast to more hemispherical low-density bubbles observed under the irradiation by a 150-ns pulse. The behavior of the nascent bubbles is consistent with the behavior of the later plasma in the bubbles, which is crucial for observation of well-defined atomic spectral lines for underwater LIBS.

Key words:

underwater LIBS, cavitation bubble, laser pulse width, long pulse, liquid-phase laser ablation

1. Introduction

Laser induced breakdown spectroscopy (LIBS) has great potential for application to *in situ* elemental analysis in various underwater situations [1-5]. In particular, the application to deep-sea exploration [6-8] could offer significant reductions in cost by increasing efficiency over traditional sampling-based survey methods. The main advantages of LIBS are the feasibility of remote sensing [7], high sensitivity to most elements in the periodic table, and the applicability to various states of samples [9]. However, underwater LIBS measurements suffer complications due to the confinement of the plasma to a small volume [10], i.e., it is difficult to obtain a plasma of low-density and high-temperature. The emission spectra are significantly deformed by collisions and Stark broadening [11,12] and suffer from self-absorption [13,14]. It is known that irradiation of a laser pulse underwater forms a cavitation bubble [15-20], and it is thought that the timing of bubble formation and growth relative to the plasma generation is a key factor that strongly influences the quality of underwater LIB spectra [15,21].

Attempts to control this timing have been performed by changing the irradiation scheme. It seems that the timing of the plasma formation relative to the bubble formation can be controlled by double-pulse irradiation, which is known to give high quality spectra with the broadening of atomic spectral lines being significantly suppressed [15,22,23]. We have previously demonstrated that optimization of double-pulse irradiation parameters can yield high quality spectra with non-gated detection scheme, if both the pulse interval and pulse energy are optimized [21]. Optimization of the pulse interval, in this case, is equivalent to the optimization of the timing of the plasma formation relative to the bubble generation, since in the optimized condition the first pulse takes charge in the creation of a bubble without the generation of a plasma, while the second pulse generates a low density plasma in the bubble formed by the first pulse [21].

Although the double-pulse irradiation scheme is successful in obtaining well-defined spectra for underwater LIBS, the deformation of atomic line spectra is pronounced when the hydrostatic pressure becomes more than 10 MPa [8] or 5 MPa [24] corresponding to a depth of 1000 m or 500 m, respectively. It is known that the bubble growth is restricted at even slightly elevated pressures, and does not seem to

offer any advantage over single pulse irradiation when the plasma is generated by the second pulse [20, 24].

The irradiation of a single long pulse (~150 ns) is also known to give clear atomic emission line spectra [25]. In this irradiation scheme a pulse energy of several millijoules gives sufficiently intense optical emission for LIBS measurements, and has an advantage of lower damage to the target [26] as well as a simpler instrumentation. On the analogy of the double-pulse irradiation, the mechanism leading to the well-defined clear spectra in this case is explained by the plasma emission lasting until the bubble becomes sufficiently developed [10]. In order to verify this explanation, and clarify the phenomena more in detail, it is important to investigate the timing of bubble formation for the long-pulse irradiation scheme. The formation mechanism of the bubble is also important in view of the application to a high hydrostatic pressure environment, where the bubble growth is strongly suppressed and the double-pulse mechanism no longer works, while a single pulse is essentially not affected by the external hydrostatic pressure, and a long single pulse still gives well-defined clear line spectra [6,27].

In the present work, we examine the timing of the bubble formation by shadowgraphy using monochromatic back illumination in combination with an interference filter to remove the intense emission of the plasma. Since the nascent bubble is very small, a microscope was used for the shadowgraphy. An intensified charge coupled device (ICCD) was used as the camera for the shadowgraphy to attain a 5-ns temporal resolution. The experiments were performed by irradiating the target with two different pulse widths, 20-ns pulse (short pulse) and 150-ns pulse (long pulse). The formation of the bubble takes place during the leading edge of the long, 150-ns, pulse, and later, the bubble grows sufficiently for the plasma to be entirely included in the bubble. Timing of the bubble formation was also investigated in case of irradiation with a short, 20-ns, pulse, and a comparison was made with the observations for the long pulse. We also discuss the reason why spectral features depend on the pulse width, i.e., a long pulse gives well-defined clear line spectra [25], while a short pulse usually results in a considerably deformed spectra.

2. Experiment

The experimental setup is schematically shown in Fig. 1. The fundamental wavelength (1064 nm) of a flash-lamp-pumped Q-switched Nd:YAG laser (home built) was used as the ablation laser. The pulse width is 20 ns under normal operating conditions. A pulse width as long as 150 ns is obtained by lowering the power of the flashlamp to near the lasing threshold [25]. Since only a low energy pulse can be achieved when operating the laser in this manner, the output from the laser oscillator is passed through an optical amplifier to give a pulse energy sufficient for ablation. A pulse energy of 12 mJ was used for the 20-ns pulse, while 2 mJ was used in case of the 150-ns pulse width. Different pulse energies were used since they are the energies giving the highest quality spectra. A small portion of the laser pulse was introduced into a fast photodiode (PD1) to trigger the ICCD (Princeton, PI-MAX:1K) for shadowgraphy. The remaining part of the laser passed through a 50 ns optical delay. The laser beam was then focused with a 60-mm focal-length lens, and a target in a water cell was irradiated at the focal point. Just before the irradiation, a portion of the pulse was introduced into a fast photodiode (PD2), the signal of which gives the temporal profile of the laser pulse, and was recorded by an oscilloscope. Although the pulser to drive the ICCD has an internal delay of ~50 ns from the trigger to the output of an electrical pulse which drives the ICCD gate, the optical delay of the laser pulse enables us to capture a shadowgraph image at the very beginning of the pulse. The high-voltage electrical pulse from the pulser, which determines the time-gate of the measurement, was monitored by the same oscilloscope as used to monitor the pulse profile.

The shadowgraph was observed by the ICCD detector via a water immersion type microscope objective lens with a magnification of 40x (Olympus, LUMPlanFL), together with an imaging lens. The objective lens was dipped in water through a hole made in the side of the irradiation cell. The ICCD detector was operated with a gate width of 5 ns. A frequency doubled Nd:YAG laser (home built) was used for the back illumination. The pulse width of this laser was ~20 ns. The intensity of the laser was regulated with a variable neutral-density (ND) filter, and then the laser was scattered by a diffuser made of acrylic resin. An interference filter (532 nm) was placed in front of the ICCD detector in order to block the spontaneous emission from the plasma, and only 532 nm light was detected. The timing of the illumination laser with respective to the ablation laser was controlled by a delay generator (Stanford Research Systems,

DG535).

The cell was rectangular and made of polytetrafluoroethylene resin. It has two windows in the sides, one for ablation laser and the other for the back illumination for shadowgraphy, and one hole to attach a microscope objective lens. The target was a Cu plate (Nilaco) polished using emery paper. It was placed in the cell, and the cell was filled with pure water.

Atomic lines of the Cu I $^2S_{1/2}$–$^2P^o_{3/2}$ ($^2P^o_{1/2}$) fine-structure doublet were observed after irradiation with three different pulse widths, i.e., 20 ns, 50 ns, and 100 ns. The same target Cu plate used for shadowgraphy was placed in pure water (Millipore, Milli-Q). A pulse of energy 5.4 mJ was focused onto the target by a plano-convex lens with a focal length of 70 mm. The gate delay was 600 ns from the rising edge of the pulse, and the gate width was 100 ns in case of the irradiation with a 20 ns pulse, and 1000 ns for the other cases. The emission was observed from the lateral direction, and collected by two plano-convex lenses with a focal length of 70 mm, and then introduced into an optical fiber bundle. The end of the fiber was attached to the entrance slit of a spectrograph (Bunkoukeiki, MK-302) equipped with 1200-groove/mm grating as well as an ICCD detector (Princeton Instruments, ICCD-1024MTDGE/1).

3. Results and discussion

Shadowgraphs of nascent cavitation bubbles were successfully obtained with nanosecond time resolution and high magnification. Typical results are shown in Figs. 2 and 3. Since the laser pulse was used for the back illumination, features due to interference are unavoidable in the bright region in the image. Nevertheless, clear images of nascent cavitation bubbles can be observed. The timing of the shadowgraph measurement as well as the laser pulse profile is seen in the oscilloscope chart (Figs. 2(a) and 3(a)) shown above each shadowgraph. Figs. 2(b1) to (b4) are the shadowgraphs obtained at -120 ns, -63 ns, 29 ns, 297 ns relative to the peak of 150-ns pulse, and Figs. 3(b1) to (b4) are those obtained at -9 ns, 7 ns, 40 ns, 81 ns relative to the peak of the 20-ns pulse.

A nascent bubble is seen in Fig. 2(b1) at 120 ns before the peak of the 150-ns pulse. As can be seen in Fig. 2(a1) the timing of the shadowgraph image corresponds to the rising edge of the pulse. This suggests that a tiny portion of the pulse energy is

enough to generate the bubble. At 63 ns before the peak of the pulse (Fig. 2(a2)), the bubble is as large as ~20 μm in the direction normal to the surface, and its boundary with water is clearly seen with a contact angle smaller than 90 degrees. The boundary is not perfectly smooth, but has a bumpy structure. Later at 29 ns after the peak of the pulse (Fig. 2(a3)) the bubble is more hemispherical and the contact angle is closer to 90 degrees. Note that at this timing the intensity of the laser pulse is still comparable to the peak intensity. Later, 297 ns after the peak of the pulse (Fig. 2(a4)) the bubble is hemispherical with the radius as large as ~130 μm. In the bubble some light is seen. We think that this is due to a scattering of light by a small roughness of the bubble boundary, although it looks smooth in the shadowgraph. Smaller bubbles at earlier delay times do not show any light in the bubble, probably because the light is intensively scattered at the bubble surface, and does not penetrate into the bubble. In Fig. 2(b3) shock wave propagation is seen as a dark half ring. The observation of the shock, however, was not stable in the case of the long-pulse irradiation.

The shadowgraph obtained 9 ns before the peak of the 20-ns pulse is shown in Fig. 3(b1). Shock wave propagation is seen as a dark half ring and optical emissions from the ablated material are seen near the target surface. Although the interference filter transmits only ~3 nm band-width around 532 nm, the emission exceeds the back illumination and the cavitation bubble is not clearly seen in the shadowgraph. Looking at the image carefully, a shadow can be seen at both sides of the plasma, which are thought to be the edges of the bubble. In the direction normal to the surface the emission region seems to exceed the bubble region expected from the observed edges. The boundary between the plasma and water is not clear, meaning a gradual density gradient between the plasma and water. The contact angle estimated from the shadow of the bubble edges is considerably smaller than 90 degrees. It seems that the bubble is pretty flat and filled with dense matter, which probably originates from the ablated species as well as originating from water in the liquid phase adjacent to this region. A shadowgraph obtained at 7 ns after the peak of the 20-ns pulse is shown in Fig. 3(b2). Although the shock wave and the bubble size are larger than in Fig. 3(b1), the shadowgraph obtained at this timing was qualitatively the same as in Fig. 3(b1). Note that the intensity of the laser pulse is still considerably high at this time. At 40 ns after the peak of the laser pulse (Fig. 3(b3)), the optical emission is no longer observed, and the bubble boundary is clearly seen. The shape of the bubble is flat and the contact

angle is small. At 81 ns from the peak of the laser pulse (Fig. 3(b4)) the contact angle becomes larger and the shape of the bubble becomes comparatively hemispherical.

The present results show that the generation of the cavitation bubble occurs during the leading edge of laser pulse profiles, regardless of the pulse width. However, the images of nascent bubbles shown in Figs. 2(a1), 2(a2) and 3(a1) are quite different. The intense optical emission observed in case of short-pulse irradiation suggests a high temperature and high density in this region, which is caused by a large amount of ablated material supplied immediately after or simultaneous with the bubble generation. Note that a short pulse is known to ablate more material than a long pulse [17,26]. The small bubble size at the time of an explosive ablation also makes the ablated material extremely dense. Excitation energy is also confined into a small region, which causes an intense emission. Although we see a trace of bubble boundary at the edge of the bubble, the dense plasma seems to have direct contact with or to be integrated with water. This close contact dissipates the excitation energy into liquid phase, and results in a fast quenching of the optical emission. In case of a long-pulse irradiation, on the other hand, the emission intensity from the ablated species is low and cannot be observed in the present experimental setup throughout the time range of the measurement. The optical emission at much later delay times, such as 400 ns, observed in our previous shadowgraph measurement, show that the long-pulse irradiations give more intense emission than short pulse [17]. This is in contrast to the present results. Although we are using higher pulse energy for the short pulse than the long pulse, we think that the results are explained from the view point of different behavior of the density in the bubble due to the pulse width. In case of a long-pulse irradiation, only a small portion of the pulse energy has been deposited onto the target surface at the timing when the bubble size is small, and hence, only a small amount of ablated material is in the bubble. Since the remaining portion of the pulse energy is given to the continuously growing bubble and material removal from the target surface is only gradual, the ablated species cannot be as dense as in the case of short-pulse irradiation. Furthermore, our previous results of the crater depth measurements suggest that the amount of material removal is rather small in case of a long-pulse irradiation [26], indicating that the energy of the later portion of the pulse is mostly given to the plasma and not used for the ablation, which is favorable for the formation of low density plasma in the bubble.

A distinguishing feature of the nascent bubbles obtained by short- and

long-pulse irradiations is the contact angle of the bubble. At the equilibrium the contact angle θ is determined by the Young equation, $\gamma_{SL}=\gamma_{SB}+\gamma_{LB}\cos\theta$, where γ_{SL}, γ_{SB}, and γ_{LB} are interfacial tensions of solid/liquid, solid/bubble, and liquid/bubble interfaces, respectively. The small contact angle of the nascent bubbles obtained by short-pulse irradiation suggests a lower γ_{SB} and γ_{LB} compared with long-pulse irradiation, and hence suggests that the bubbles generated by short-pulse irradiation are more dense than for long-pulse irradiation. This is consistent with the above discussion that the optical emission in nascent bubbles obtained with a short-pulse irradiation is assigned to highly dense matter characteristic to the short-pulse irradiation.

We have previously demonstrated that the long-pulse irradiation is advantageous for underwater LIBS from the view point of obtaining well-defined atomic spectral lines [25]. In Fig. 4 Cu atomic lines of the transition Cu I $^2S_{1/2} - {}^2P^o_{3/2}$ ($^2P^o_{1/2}$) (fine-structure doublet) obtained with three different pulse widths, namely 20 ns, 50 ns, and 100 ns, are shown. It is clearly seen that the spectra obtained with shorter-pulse irradiations suffer from low intensity and serious spectral deformation, which has been attributed to intense self-absorption and spectral broadening caused by high density in the light-emitting region. On the other hand the long-pulse irradiation gives clear spectral lines with less degradation of the signal through self-absorption. The present results of the nascent-bubble images seem to give an explanation for the advantage of the long-pulse irradiation. The features of the image in the case of short-pulse irradiation are all explained by a high density in the nascent bubble. The intense excitation in a very short time range in a nascent bubble is not effectively kept in the bubble, since the excitation is quenched by the surrounded water. As a result, after the expansion of the bubble, the excitation in the bubble is not sufficient for the LIBS measurement. With long-pulse irradiation, however, excitation continues until the bubble grows to be sufficiently large. This results in low-density plasma in the expanded bubble, which gives well-defined atomic spectral lines for underwater LIBS.

4. Conclusions

We have observed nascent cavitation bubbles obtained by irradiation of Cu target in water with the different laser pulse widths of 20 ns and 150 ns. The 20-ns pulse gives a

flat bubble filled with intense emission during the laser pulse, while 150-ns pulse gives hemispherical bubble from the very beginning without optical emission observable in the present experimental setup. These features of the bubble images are all explained by a high plasma density in the small nascent bubble in case of short-pulse irradiation, and comparatively low density even in a very nascent bubble obtained for the long-pulse irradiation. With the long-pulse irradiation the excitation of the plasma is rather gradual, and hence, it is suitable to obtain highly-excited low-density plasma at the delay time of several hundreds of nanosecond, which is the timing of typical underwater LIBS measurements. The information obtained in the present work is useful for further optimization of the irradiation parameters, such as pulse width or pulse energy, for various irradiation schemes.

Acknowledgment

One of the authors (TS) would like to thank Dr. A. De Giacomo for fruitful discussion. This work was financially supported by JSPS KAKENHI Grant Number 23560023.

References

[1] A. De Giacomo, M. Dell'Aglio, O. De Pascale, M. Capitelli, From single pulse to double pulse ns-laser induced breakdown spectroscopy under water: Elemental analysis of aqueous solutions and submerged solid samples, Spectrochim. Acta Part B 62 (2007) 721-738.

[2] V. Lazic, F. Colao, R. Fantoni, V. Spizzicchino, Recognition of archeological materials underwater by laser induced breakdown spectroscopy, Spectrochim. Acta Part B 60 (2005) 1014-1024.

[3] V. Lazic, F. Colao, R. Fantoni, V. Spizzichino, S. Jovicevic, Underwater sediment analyses by laser induced breakdown spectroscopy and calibration procedure for fluctuating plasma parameters, Spectrochim. Acta Part B 62 (2007) 30–39.

[4] T. Nishi, T. Sakka, H. Oguchi, K. Fukami, Y. H. Ogata, In situ electrode surface analysis by laser-induced breakdown spectroscopy, J. Electrochem. Soc. 155 (2008) F237-F240.

[5] T. Sakka, S. Iwanaga, Y. H. Ogata, A. Matsunawa, T. Takemoto, Laser ablation at solid–liquid interfaces: An approach from optical emission spectra, J. Chem. Phys. 112 (2000) 8645-8653.

[6] B. Thornton, T. Ura, Effects of pressure on the optical emissions observed from solids immersed in water using a single pulse laser, Appl. Phys. Express 4 (2011) 022702.

[7] B. Thornton, T. Masamura, T. Takahashi, T. Ura, K. Ohki, T. Sakka, Development and field testing of laser-induced breakdown spectroscopy for in situ multi-element analysis at sea, Oceans2012 (2012).

[8] M. Lawrence-Snyder, J. Scaffidi, S. M. Angel, A. P. M. Michel, A. D. Chave, Sequential-pulse laser-induced breakdown spectroscopy of high-pressure bulk aqueous

solutions, Appl. Spectrosc. 61 (2007) 171-176.

[9] D. A. Cremers and L. J. Radziemski, History and fundamentals of LIBS, in: A.W. Miziolek, V. Palleschi, I. Schechter (Eds.), Laser Induced Breakdown Spectroscopy, Cambridge University Press, Cambridge, 2006, pp. 1-39.

[10] H. Oguchi, T. Sakka, Y. H. Ogata, Effects of pulse duration upon the plume formation by the laser ablation of Cu in water, J. Appl. Phys. 102 (2007) 023306.

[11] H. R. Griem, Plasma Spectroscopy, McGraw–Hill, New York, 1964.

[12] H. R. Griem, Principles of Plasma Spectroscopy, Cambridge University Press, Cambridge, 1997.

[13] T. Sakka, K. Takatani, Y. H. Ogata, M. Mabuchi, Laser ablation at the solid–liquid interface: Transient absorption of continuous spectral emission by ablated aluminium atoms, J. Phys. D: Appl. Phys. 35 (2002) 65–73

[14] T. Sakka. T. Nakajima. Y. H. Ogata, Spatial population distribution of laser ablation species determined by self-reversed emission line profile, J. Appl. Phys. 92 (2002) 2296-2303.

[15] A. E. Pichahchy, D. A. Cremers, M. J. Ferris, Elemental analysis of metals under water using laser-induced breakdown spectroscopy, Spectrochim. Acta Part B 52 (1997) 25-39.

[16] T. Tsuji, Y. Tsuboi, N. Kitamura, M. Tsuji, Microsecond-resolved imaging of laser ablation at solid-liquid interface: Investigation of formation process of nano-size metal colloids, Appl. Surf. Sci. 229 (2004) 365-371.

[17] T. Sakka, S. Masai, K. Fukami, Y. H. Ogata, Spectral profile of atomic emission lines and effects of pulse duration on laser ablation in liquid, Spectrochim. Acta Part B 64 (2009) 981-985.

[18] K. Sasaki, T. Nakano, W. Soliman, N. Takada, Effect of pressurization on the dynamics of a cavitation bubble induced by liquid-phase laser ablation, Appl. Phys. Express 2 (2009) 046501.

[19] W. Soliman, T. Nakano, N. Takada, K. Sasaki, Modification of Rayleigh-Plesset theory for reproducing dynamics of cavitation bubbles in liquid-phase laser ablation, Jpn. J. Appl. Phys. 49 (2010) 116202.

[20] B. Thornton, T. Takahashi, T. Ura, T. Sakka, Cavity formation and material ablation for single-pulse laser-ablated solids immersed in water at high pressure, Appl. Phys. Express 5 (2012) 102402.

[21] T. Sakka, A. Tamura, T. Nakajima, K. Fukami, Y. H. Ogata, Synergetic effects of double laser pulses for the formation of mild plasma in water: Toward non-gated underwater laser-induced breakdown spectroscopy, J. Chem. Phys. 136 (2012) 174201.

[22] R. Nyga, W. Neu, Double-pulse technique for optical emission spectroscopy of ablation plasmas of samples in liquids, Opt. Lett. 18 (1993) 747-749.

[23] A. De Giacomo, M. Dell'Aglio, A. Casavola, G. Colonna, O. De Pascale, M. Capitelli, Elemental chemical analysis of submerged targets by double-pulse laser-induced breakdown spectroscopy, Anal. Bioanal. Chem. 385 (2006) 303-311.

[24] T. Takahashi, B. Thornton, T. Ura, Investigation of influence of hydrostatic pressure on double-pulse laser-induced breakdown spectroscopy for detection of Cu and Zn in submerged solids, Appl. Phys. Express 6 (2013) 042403

[25] T. Sakka, H. Oguchi, S. Masai, K. Hirata, Y. H. Ogata, M. Saeki, H. Ohba, Use of a long-duration ns pulse for efficient emission of spectral lines from the laser ablation plume in water, Appl. Phys. Lett. 88 (2006) 061120.

[26] T. Sakka, H. Oguchi, S. Masai, Y. H. Ogata, Quasi nondestructive elemental

analysis of solid surface in liquid by long-pulse laser ablation plume spectroscopy, Chem. Lett. 36 (2007) 508-509.

[27] B. Thorntona, T. Sakka, T. Takahashi, A. Tamura, T. Masamura, A. Matsumoto, Spectroscopic measurements of solids immersed in water at high pressure using a long-duration nanosecond laser pulse, Appl. Phys. Express 6 (2013) 082401.

Figure captions

Fig. 1. Experimental setup.

Fig. 2. Shadowgraph image of the cavitation bubble in case of the laser pulse width of 150 ns. In (a) the gate timing of the shadowgraph acquisition (blue line) with respect to laser pulse profile (red line) is indicated. In (b) shadowgraphs obtained at different gate timings are shown. The timing of each image corresponds to the timing indicated in the chart above each image. Figs. 2(b1) to (b4) are the shadowgraphs obtained at -120 ns, -63 ns, 29 ns, 297 ns relative to the peak of the pulse.

Fig. 3. Shadowgraph image of the cavitation bubble in case of the laser pulse width of 20 ns. In (a) the gate timing of the shadowgraph acquisition (blue line) with respect to laser pulse profile (red line) is indicated. In (b) shadowgraphs obtained at different gate timings are shown. The timing of each image corresponds to the timing indicated in the chart above each image. Figs. 3(b1) to (b4) are the shadowgraphs obtained at -9 ns, 7 ns, 40 ns, 81 ns relative to the peak of the pulse

Fig. 4. Emission spectra obtained by the irradiation with three different pulse widths. The target was Cu plate placed in pure water. The pulse energy was 5.4 mJ, and the pulse width was (a) 20 ns, (b) 50 ns, and (c) 100 ns. The gate delay was 600 ns from the rising edge of the pulse, and the gate width was (a) 100 ns, (b) 1000 ns, and (c) 1000 ns.

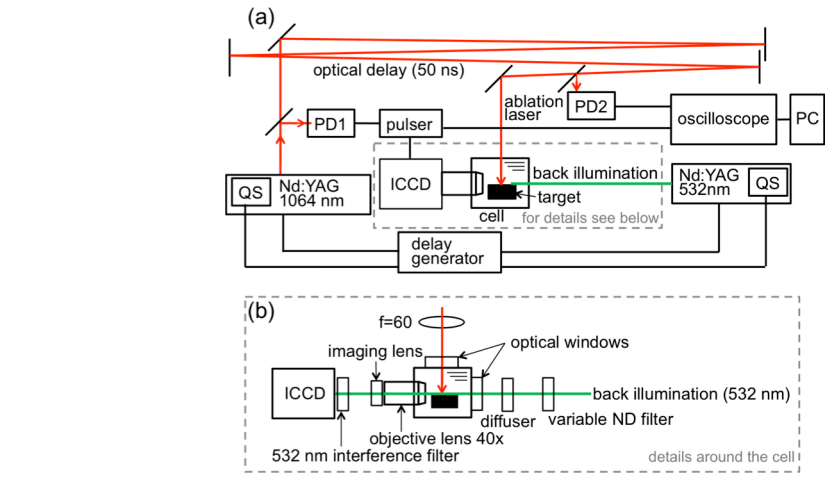

Fig. 1. Experimental setup.

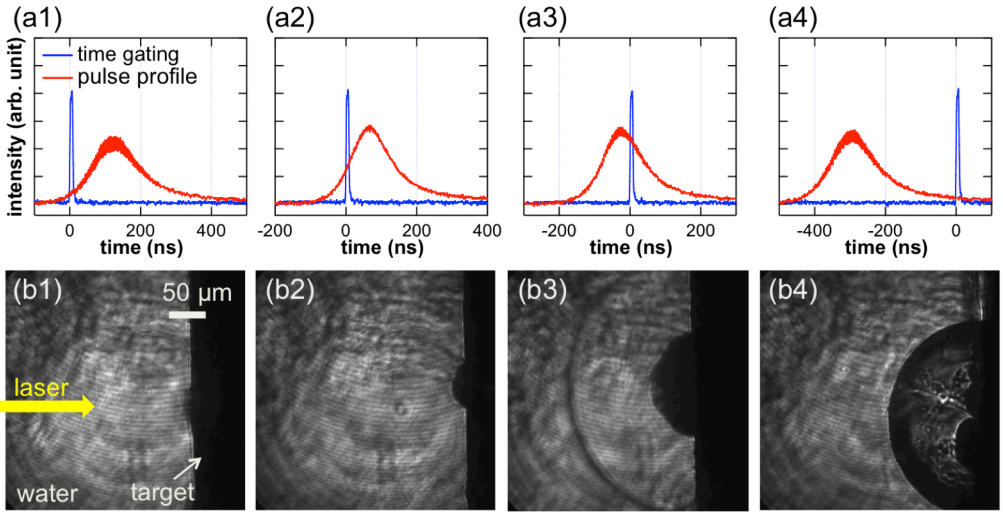

Fig. 2. Shadowgraph image of the cavitation bubble in case of the laser pulse width of 150 ns. In (a) the gate timing of the shadowgraph acquisition (blue line) with respect to laser pulse profile (red line) is indicated. In (b) shadowgraphs obtained at different gate timings are shown. The timing of each image corresponds to the timing indicated in the chart above each image. Figs. 2(b1) to (b4) are the shadowgraphs obtained at -120 ns, -63 ns, 29 ns, 297 ns relative to the peak of the pulse.

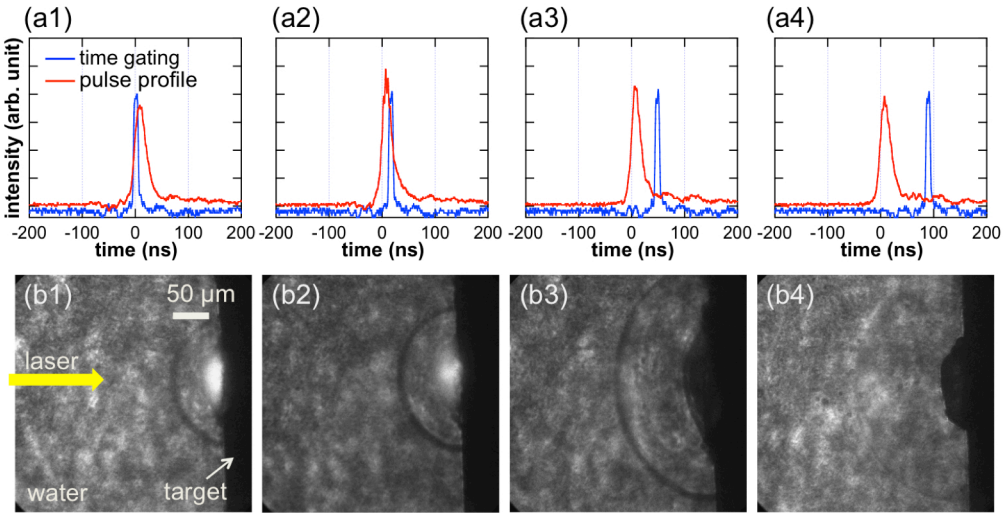

Fig. 3. Shadowgraph image of the cavitation bubble in case of the laser pulse width of 20 ns. In (a) the gate timing of the shadowgraph acquisition (blue line) with respect to laser pulse profile (red line) is indicated. In (b) shadowgraphs obtained at different gate timings are shown. The timing of each image corresponds to the timing indicated in the chart above each image. Figs. 3(b1) to (b4) are the shadowgraphs obtained at -9 ns, 7 ns, 40 ns, 81 ns relative to the peak of the pulse

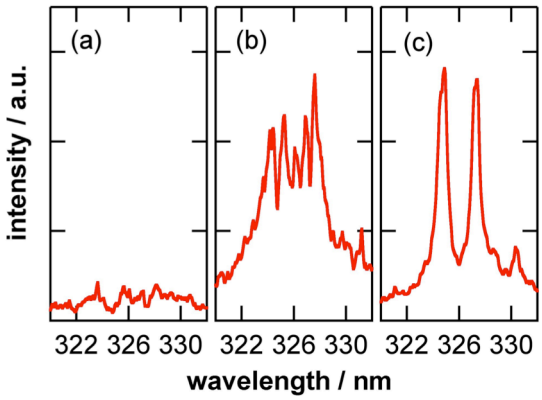

Fig. 4. Emission spectra obtained by the irradiation with three different pulse widths. The target was Cu plate placed in pure water. The pulse energy was 5.4 mJ, and the pulse width was (a) 20 ns, (b) 50 ns, and (c) 100 ns. The gate delay was 600 ns from the rising edge of the pulse, and the gate width was (a) 100 ns, (b) 1000 ns, and (c) 1000 ns.